Electronic Supplementary Material (ESI) for Journal of Materials Chemistry A.
This journal is © The Royal Society of Chemistry 2019

Supporting Information

Porous $CuBi_2O_4$ Photocathodes with Rationally Engineered Morphology and Composition towards Photoelectrochemical Water Splitting

Youxun Xu,[a] Jie Jian,[a] Fan Li,[a] Wei Liu,[a] Lichao Jia,[*b] and Hongqiang Wang[*a]

[a]*State Key Laboratory of Solidification Processing, Center for Nano Energy Materials, School of Materials Science and Engineering, Northwestern Polytechnical University and Shaanxi Joint Labortary of Graphene, Xi'an, 710072, P. R. China.*

[b]*Key Laboratory of Applied Surface and Colloid Chemistry, National Ministry of Education, Shaanxi Key Laboratory for Advanced Energy Devices, Shaanxi Engineering Lab for Advanced Energy Technology, School of Materials Science and Engineering, Institution Shaanxi Normal University, Address 2620 West Chang'an Street, Xi'an, Shaanxi, 710119, China.*

† *E-mail: hongqiang.wang@nwpu.edu.cn; lichaojia@snnu.edu.cn*

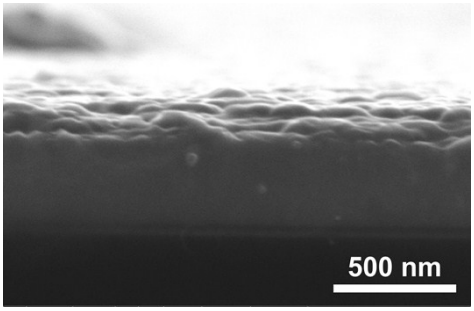

Figure S1. Cross sectional SEM image of the $CuBi_2O_4$ film by spin coating 0.15 M precursor solution with no F-108 (CBO).

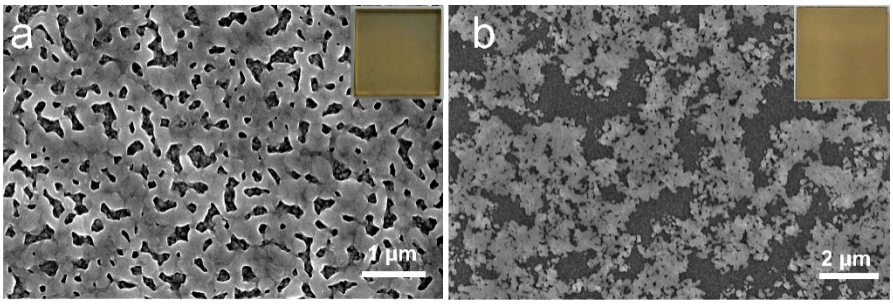

Figure S2. SEM images of $CuBi_2O_4$ film by spin coating 0.15 M precursor solution with (a) 0.05 mg/ml F-108 (CBO-F-108-1) and (b) 0.25 mg/ml F-108 (CBO-F-108-1).

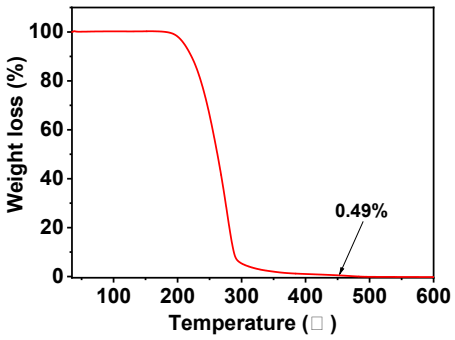

Figure S3. TG curve of F-108.

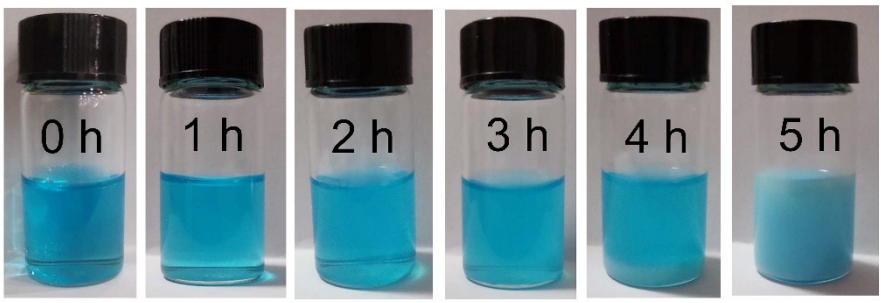

Figure S4. Photographs of precursor solution with ethanol and acetic acid (2:1 by volume) aging for different time of periods.

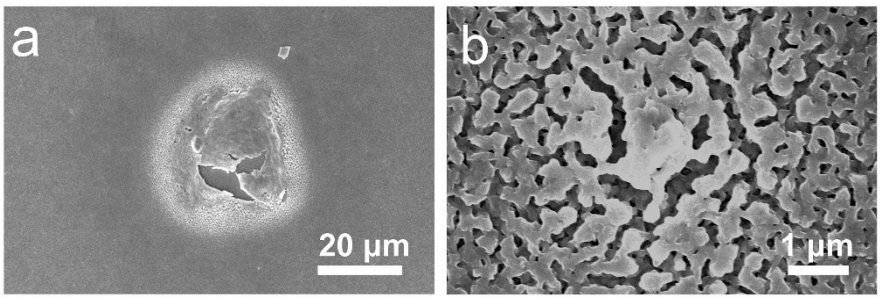

Figure S5. SEM images of uneven $CuBi_2O_4$ films by spin coating hydrolyzed precursor solution.

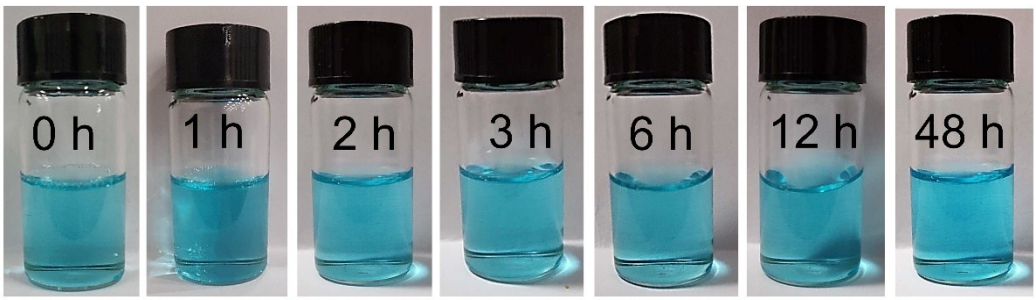

Figure S6. Photographs of precursor solution with 35% ethylene glycol by volume aging for different time of periods.

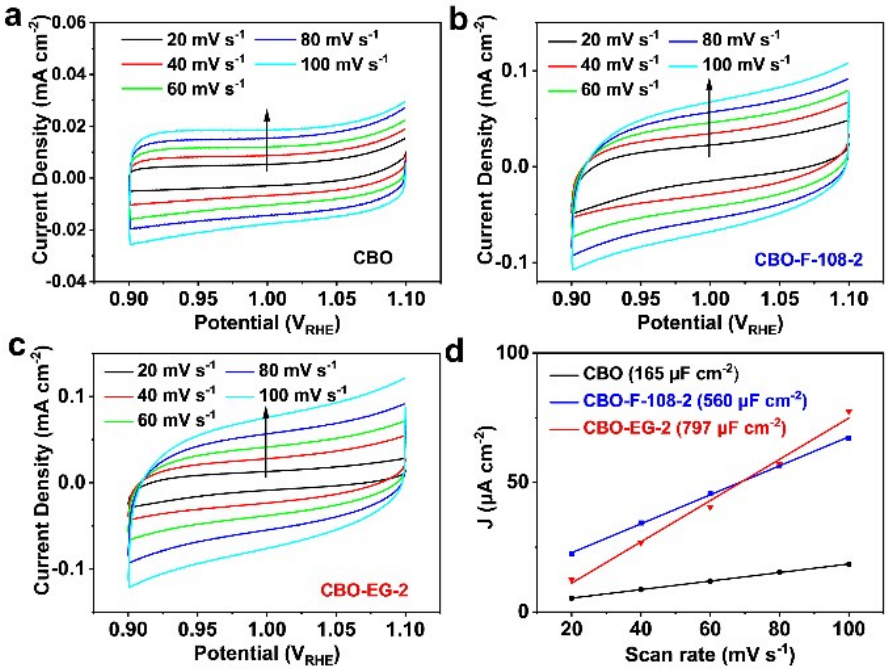

Figure S7. Cyclic voltammetry curves of (a) CBO (no F-108, no EG), (b) CBO-F-108-2 and (c) CBO-EG-2 photocathodes at various scan rates (20-100 mV s^{-1}). (d) Estimate of double layer capacitance to reflect the electrochemical active surface area.

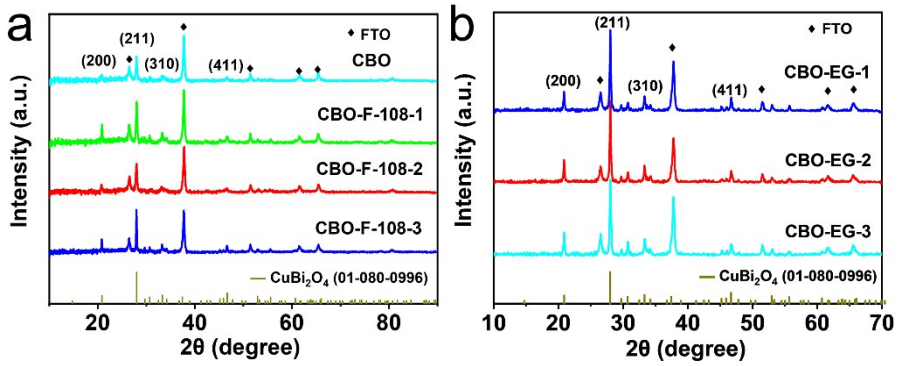

Figure S8. (a) XRD patterns of CBO (no F-108 and no EG), CBO-F-108-1, CBO-F-108-2 and CBO-F-108-3. (b) XRD patterns of CBO-EG-1, CBO-EG-2 and CBO-EG-3.

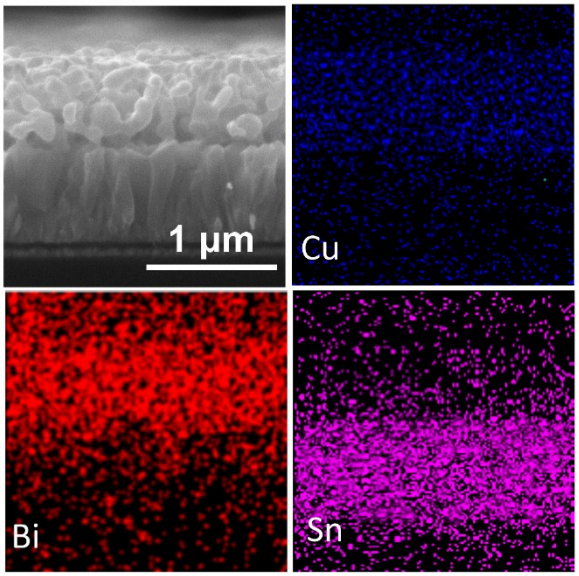

Figure S9. Cross-sectional SEM-EDS mapping of CBO-EG-2 film.

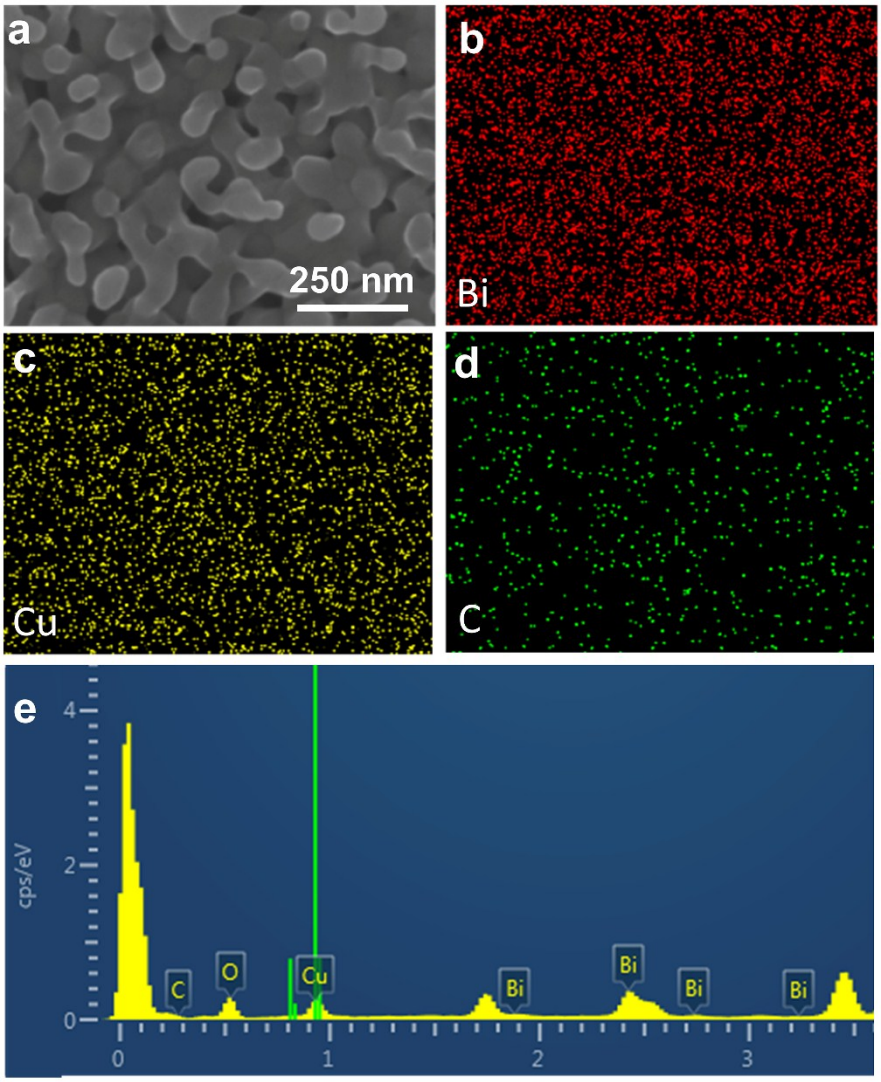

Figure S10. (a)-(d) SEM-EDS mappings of CBO-EG-2 calcining at 450 ℃ for 1h. (e) Element content distribution map of the $CuBi_2O_4$ film.

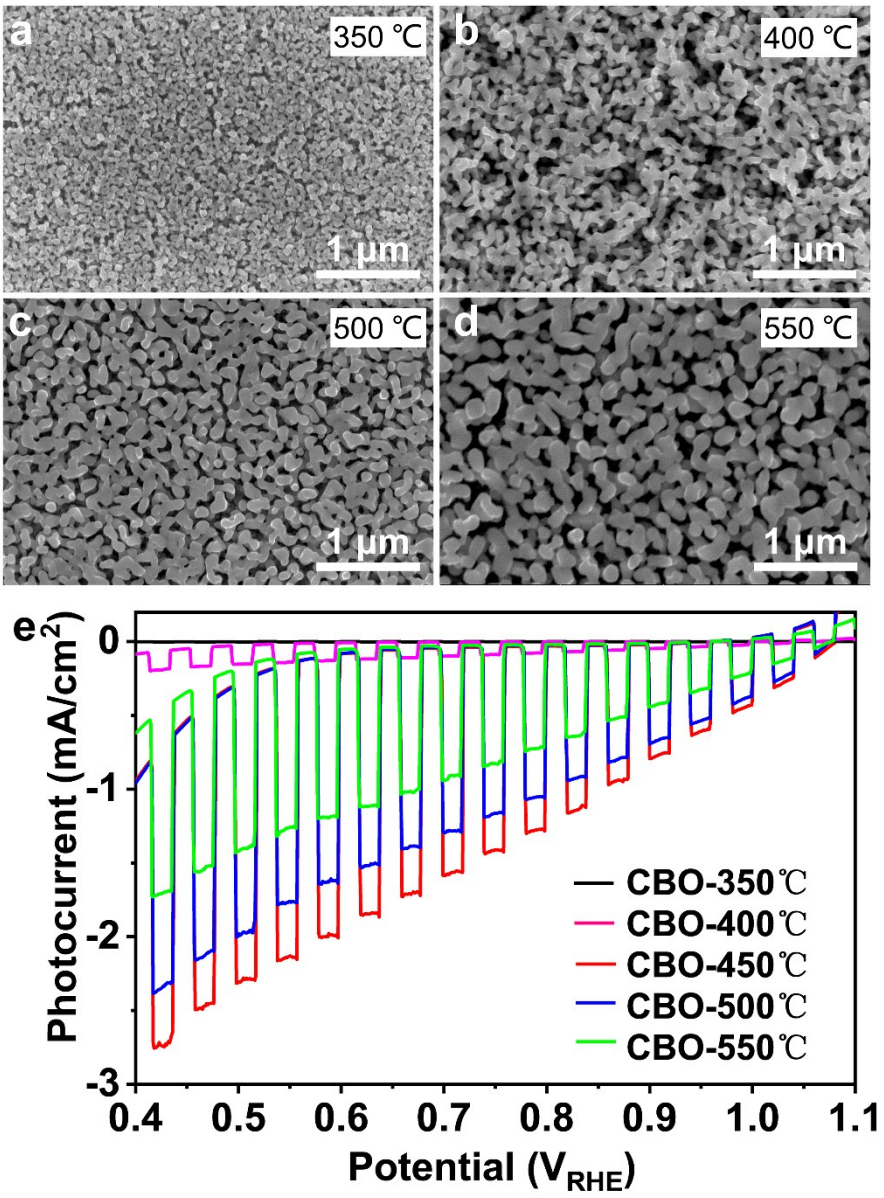

Figure S11. SEM images of nanoporous $CuBi_2O_4$ films calcined at different temperatures: (a) 350 ℃, (b) 400 ℃, (c) 500 ℃, and (d) 550 ℃. (e) Chopped LSV scans of these samples performed in 0.3 M K_2SO_4 and 0.2 M phosphate buffer (pH 6.65) with H_2O_2 back AM1.5 illumination.

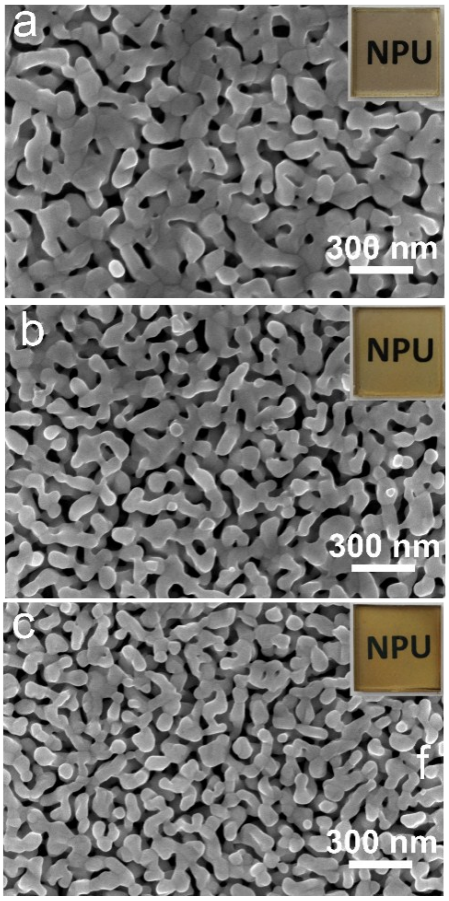

Figure S12. SEM images of nanoporous $CuBi_2O_4$ films with different thicknesses: (a) 150 nm, (b) 300 nm, and (c) 400 nm.

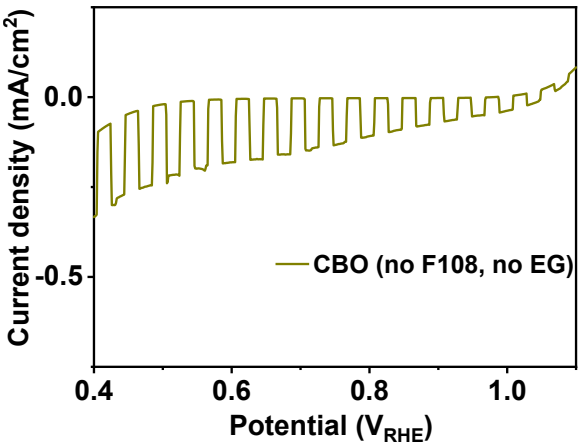

Figure S13. Chopped (light/dark) LSV scans of CBO (no F-108, no EG) performed in 0.3 M K_2SO_4 and 0.2 M phosphate buffer (pH 6.65) with H_2O_2 back AM1.5 illumination.

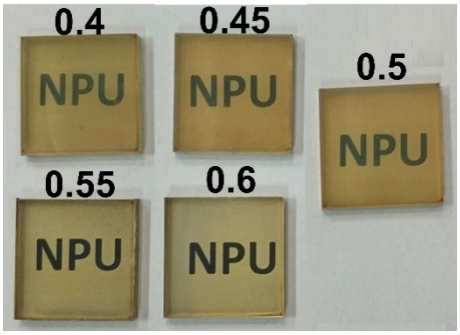

Figure S14. Digital photographs of CBO films with various Cu/Bi ratios.

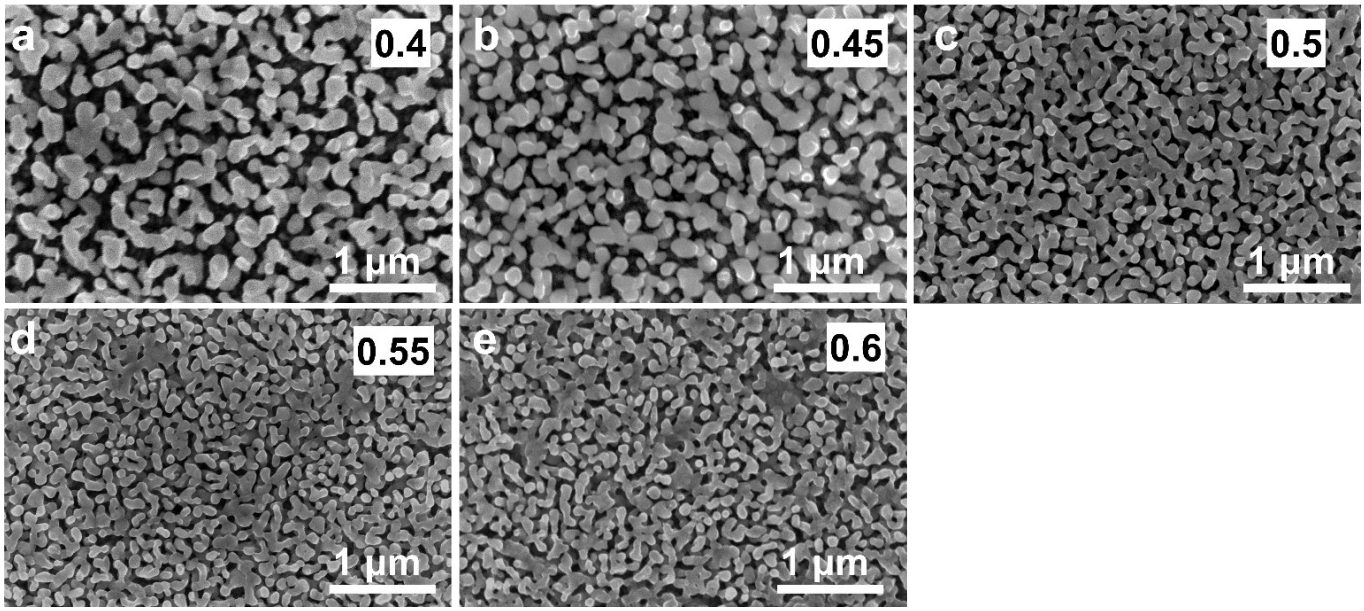

Figure S15. SEM images of CBO films with various Cu/Bi ratios.

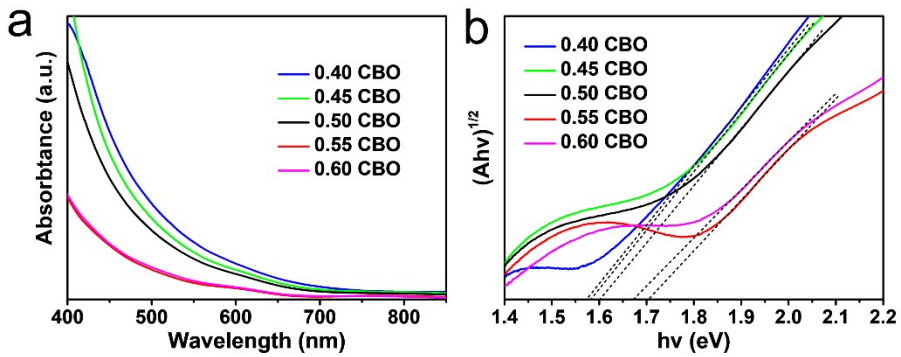

Figure S16. (a) UV/Vis absorbance spectra of CBO films with various Cu/Bi ratios. (b) Tauc plots of CBO films converted from the UV/Vis absorbance spectra. Bandgap of CBO films are 1.57, 1.58, 1.60, 1.70, and 1.67 eV for 0.40 CBO, 0.45 CBO, 0.50 CBO, 0.55 CBO, and 0.60 CBO samples.

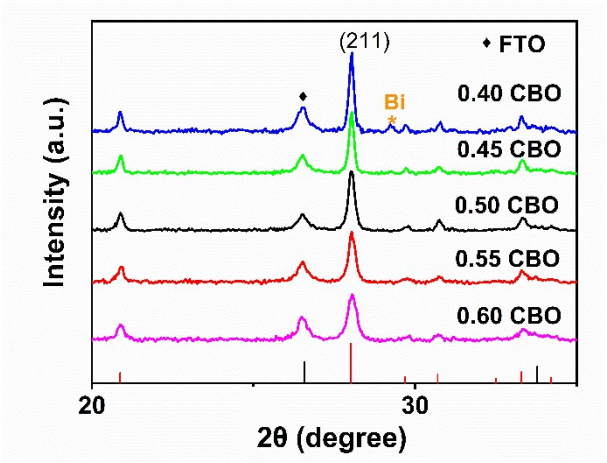

Figure S17. XRD patterns of the fabricated photocathodes.

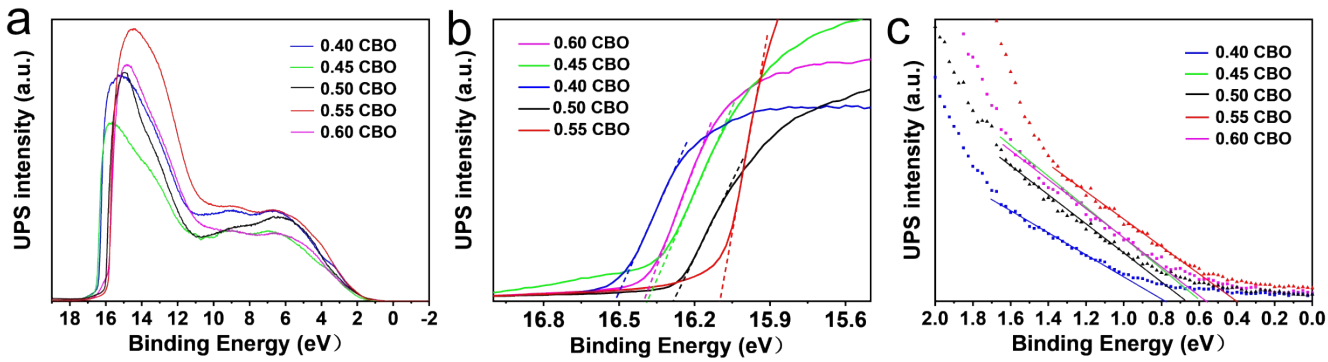

Figure S18. (a) UPS cutoff spectra for different CBO films; Magnified UPS spectra used to estimate (b) work function and (c) VBM.

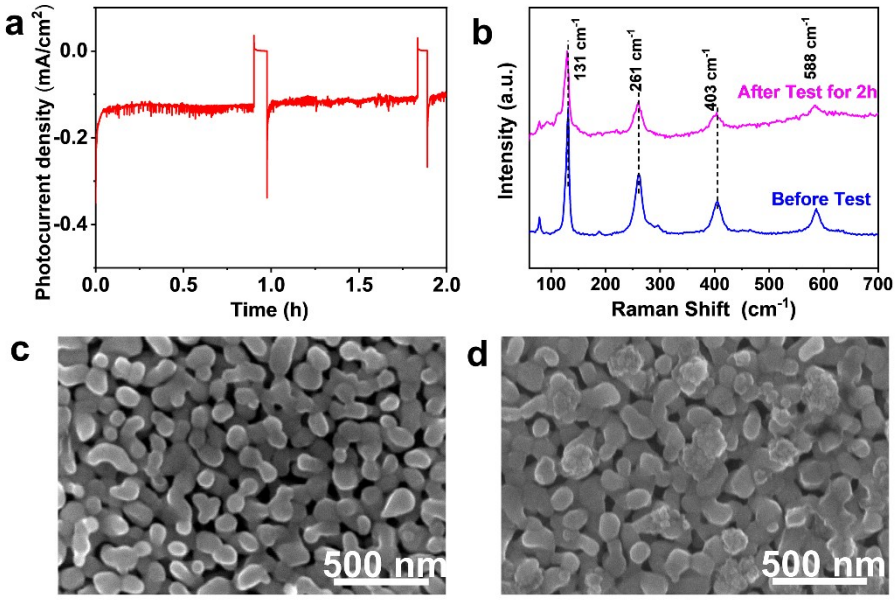

Figure S19. (a) Constant potential measurements for 0.55 CBO photocathode at 0.6 V vs RHE in 0.3 M K_2SO_4 and 0.2 M phosphate buffer (pH 6.65)， the on and off photocurrent at around 1.0 h and 2.0 h was due to the chopped illumination of the light source. (b) Raman spectra of 0.55 CBO photocathode before and after stability test. SEM images of 0.55 CBO photocathode (c) before test and (d) after test.

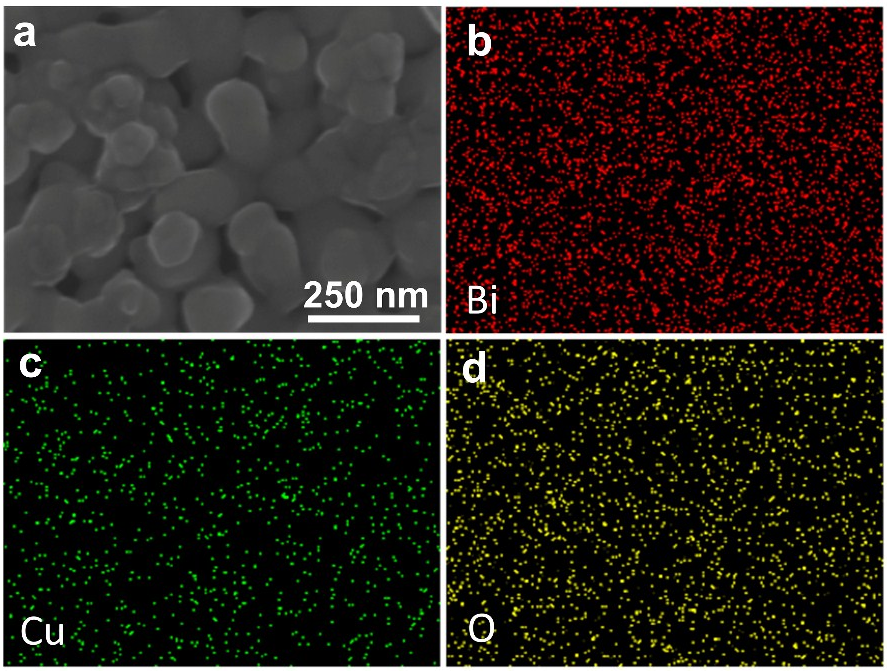

Figure S20. SEM-EDS mapping of 0.55 CBO photocathode after testing for two hours at 0.6 V vs RHE in 0.3 M K_2SO_4 and 0.2 M phosphate buffer (pH 6.65).

Table S1. Process parameters of $CuBi_2O_4$ films with different thicknesses.

Thickness	**150 nm**	**300 nm**	**400 nm**
Precursor concentration (Cu)	0.12 M	0.18 M	0.225 M
Solvent	acetic acid : ethanol : ethylene glycol 1:1:1	acetic acid : ethanol : ethylene glycol 1:1:1	acetic acid : ethanol : ethylene glycol 1:1:1
F-108	0.1 g/ml	0.2 g/ml	0.225 g/ml
Rotating speed	2000r,10s; 4500r,40s	2000r,10s; 3500r,40s	2000r,10s; 3000r,40s
Preheating temperature	150 ℃	150 ℃	125 ℃
Calcination temperature	450 ℃	450 ℃	450 ℃

Table S2. Series resistance (R_s) and charge transfer resistance (R_{ct}) of different $CuBi_2O_4$ samples.

Sample (Cu/Bi ratio)	**Rs (ohm)**	**R_{ct} (ohm)**
0.4 CBO	78	15000
0.45 CBO	80	5437
0.5 CBO	77	6132
0.55 CBO	84	4980
0.6 CBO	1980	9440

Table S3. Flat-band potential (φ_{fb}) and acceptor density (N_A) of different Cu/Bi ratio CBO samples calculated by Mott–Schottky plot.

Sample (Cu/Bi ratio)	**φ_{fb} (V_{RHE})**	**N_A (cm^{-3})**
0.4 CBO	1.31	1.7×10^{18}
0.45 CBO	1.35	2.3×10^{18}
0.5 CBO	1.31	2.4×10^{18}
0.55 CBO	1.26	4.2×10^{18}
0.6 CBO	1.31	2.5×10^{18}

Table S4. Bandgap and positions (distance from the vacuum level) of VBM (E_v), CBM (E_c), and Fermi level (E_f) of CBO samples determined by UV/Vis spectroscopy and UPS.

Sample (Cu/Bi ratio)	**E_g (eV)**	**E_v (eV)**	**E_c (eV)**	**E_f (eV)**
0.4 CBO	1.57	5.47	3.90	4.69
0.45 CBO	1.58	5.42	3.84	4.82
0.5 CBO	1.60	5.60	4.00	4.92
0.55 CBO	1.67	5.51	3.84	5.11
0.6 CBO	1.70	5.36	3.66	4.81

Table S5. Experimental results summary for the recently published $CuBi_2O_4$ photocathodes for PEC water splitting.

$CuBi_2O_4$ Photocathode	Photocurrent @ Potential (mA/cm^2)	Electrolyte	Light Source	Preparation Technique	References
CuO/ $CuBi_2O_4$/Pt	0.7 @ 0 V NHE	0.3M K_2SO_4 pH 6.8	>420nm	Drop-casting	S1
FTO/Au/ $CuBi_2O_4$/Pt	-1.24 @ 0.1V vs RHE	0.1 M Na_2SO_4 pH 6.8	AM1.5G Simulator	Cathodically electrochemical deposition	S2
Ag- $CuBi_2O_4$/Pt	1.0@0.6 V RHE	0.1 M NaOH (pH 12.8) saturated with O_2	AM1.5G Simulator	Electrodeposition	S3
$CuBi_2O_4$	2.0 @0.6 V RHE	0.3 M K_2SO_4 and 0.2 M phosphate buffer, with H_2O_2	AM1.5G Simulator	Spray pyrolysis	S4
$CuBi_2O_4$	0.02 @ -0.25V vs Ag/AgCl	0.3 M Na_2SO_4	100 mW/cm^2	Hydrothermal	S5
$CuBi_2O_4$/Pt	0.5 @ 0.4 V RHE	0.3 M K_2SO_4 and 0.2 M phosphate buffer	AM1.5G Simulator	Drop-casting	S6
$CuBi_2O_4$	0.07@ 0.6V vs RHE	0.1 M Na_2SO_4 adjusted pH 10.8	Xe lamp, >420nm	Electrochemical Synthesis	S7
$CuBi_2O_4$/CuO	0.28 @ -0.4V vs Ag/AgCl	0.1 M Na_2SO_4 pH 6.8	Xe lamp, 400 W	Spray-coating	S8
$CuBi_2O_4$	0.03 @ -0.4V vs Ag/AgCl	0.1 M Na_2SO_4 pH 6.8	500W Xe lamp,>420nm filter	Electrodeposition	S9
$CuBi_2O_4$	0.12@ -0.3V vs Ag/AgCl	0.5 M Na_2SO_4	AM 1.5, 100 mW cm^{-2}	Flux-mediated one-pot solution process	S10
Gradient $CuBi_2O_4$	2.5 @ 0.6V vs RHE (With H_2O_2)	0.3 M K_2SO_4 and 0.2 M phosphate buffer (H_2O_2)	AM1.5G Simulator	Spray pyrolysis	S11
Textured $CuBi_2O_4$	0.72 @ -0.6V vs Ag/AgCl	0.1 M Na_2SO_4 pH 6.8	AM1.5G Simulator	Vacuum Drop-casting	S12
Cu:NiO/$CuBi_2O_4$	2.83 @ 0.6V vs RHE	0.3 M K_2SO_4 and 0.2 M phosphate buffer (H_2O_2)	AM1.5G Simulator	Spray pyrolysis	S13
$CuBi_2O_4$ (Bi:Cu=1.5)	1.17 @ 0.58 V vs RHE	0.1 M $KHCO_3$ with 0.1 M $Na_2S_2O_8$ pH 8.2	AM1.5G Simulator	spin coating	S14
$CuBi_2O_4$	2.66 @ 0.6V vs RHE (With H_2O_2)	0.3 M K_2SO_4 and 0.2 M phosphate buffer (H_2O_2)	AM1.5G Simulator	spin coating	This work

References

S1. H. S. Park, C.-Y. Lee and E. Reisner. Photoelectrochemical reduction of aqueous protons with a CuO|$CuBi_2O_4$ heterojunction under visible light irradiation. Phys. Chem. Chem. Phys., 2014, 16, 22462- 22465.

S2. D. Cao, N. Nasori, Z. Wang, Y. Mi, L. Wen, Y. Yang, S. Qu, Z. Wang and Y. Lei. p-type $CuBi_2O_4$: an Easily Accessible Photocathodic Material for High-efficient Water Splitting. J. Mater. Chem. A., 2016, 4, 8995-9001.

S3. D. Kang, J. C. Hill, Y. Park, and K.-S. Choi. Photoelectrochemical Properties and Photostabilities of High Surface Area $CuBi_2O_4$ and Ag-Doped $CuBi_2O_4$ Photocathodes. Chem. Mater., 2016, 28, 4331-4340.

S4. F. Wang, A. Chemseddine, F. F. Abdi, R. van de Krol, S. P. Berglund. Spray pyrolysis of $CuBi_2O_4$ photocathodes: improved solution chemistry for highly homogeneous thin films. J. Mater. Chem. A., 2017, 5, 12838-12847.

S5. L. Zhu, P. Basnet, S. R. Larson, L. P. Jones, J. Y. Howe, R. A. Tripp, and Y. Zhao. Visible Light- Induced Photoeletrochemical and Antimicrobial Properties of Hierarchical $CuBi_2O_4$ by Facile Hydrothermal Synthesis. ChemistrySelect 2016, 1, 1518-1524.

S6. S. P. Berglund, F. F. Abdi, P. Bogdanoff, A. Chemseddine, D. Friedrich, and R. van de Krol. Comprehensive Evaluation of $CuBi_2O_4$ as a Photocathode Material for Photoelectrochemical Water Splitting. Chem. Mater. 2016, 28, 4231-4242.

S7. N. T. Hahn, V. C. Holmberg, B. A. Korgel, and C. Buddie Mullins. Electrochemical Synthesis and Characterization of p- $CuBi_2O_4$ Thin Film Photocathodes. J. Phys. Chem. C 2012, 116, 6459-6466.

S8. M. K. Hossain, G. F. Samu, K. Gandha, S. Santhanagopalan, J. Ping Liu, C. Janáky, and K. Rajeshwar. Solution Combustion Synthesis, Characterization, and Photocatalytic Activity of $CuBi_2O_4$ and Its Nanocomposites with CuO and α-Bi2O3. J. Phys. Chem. C 2017, 121, 8252-8261.

S9. Y. Nakabayashi, M. Nishikawa, Y. Nosaka. Fabrication of $CuBi_2O_4$ photocathode through novel anodic electrodeposition for solar hydrogen production. Electrochimica Acta, 2014, 125, 191-198.

S10. Y.-H. Choi, K. D. Yang, D.-H. Kim, K. T. Nam, S.-H. Hong. p-Type $CuBi_2O_4$ thin films prepared by flux-mediated one-pot solution process with improved structural and photoelectrochemical characteristics. Materials Letters, 2017, 188, 192-196.

S11. F. Wang, W. Septina, A. Chemseddine, F. F. Abdi, D. Friedrich, P. Bogdanoff, R. van de Krol, S. D. Tilley, and S. P. Berglund. Gradient self-doped $CuBi_2O_4$ with highly improved charge separation efficiency. J. Am. Chem. Soc., 2017, 139, 15094-15103.

S12. J. Li, M. Griep, Y. Choi and D. Chu, Photoelectrochemical overall water splitting with textured $CuBi_2O_4$ as a photocathode, Chem. Commun., 2018, 54, 3331-3334.

S13. A. Song, P. Plate, A. Chemseddine, F. Wang, F. F. Abdi, M. Wollgarten, R. van de Krol and S. P. Berglund, Cu:NiO as a hole-selective back contact to improve the photoelectrochemical performance of $CuBi_2O_4$ thin film photocathodes, J. Mater. Chem. A, 2019, 7, 9183–9194.

S14. Z. Zhang, S. A. Lindley, R. Dhall, K. Bustillo, W. Han, E. Xie, and J. K. Cooper, Beneficial CuO Phase Segregation in the Ternary p-Type Oxide Photocathode $CuBi_2O_4$, ACS Appl. Energy Mater.2019, 2, 4111-4117.